4.1 Introduction

As mentioned in chapter three, a new approach for diagnosing seven faults and normal status using the developed structure of ANN has been proposed. This chapter presents the four useful features (V-load, I-Load, Irradiance, and Temperature) (VIIT), considered in the proposed ANN, in detail. Also, the simulation results, which are collected from implementing the proposed ANN in both phases of training and testing, are mentioned in more detail in this chapter in addition to the evaluation scenario, which is followed to evaluate the performance of the proposed ANN, including all the evaluation metrics used.

4.2 Effective Features

The proposed PV model, discussed in Chapter Three, section 3.3 and mentioned in Figure (3.3), is designed using MATLAB/SIMULINK environment. This model is implemented eight times according to the healthy state, and seven types of PV faults are considered. At each time of implementation, three different irradiance values (500, 750, and 1000) and five different temperature values (15, 20, 25, 30, and 35) are considered. The V-load and I-load values are reordered in three different time events within the SIMILINK running. Thus, the total number of samples done each time is 45. Thus, the overall samples of all implementations include 360 samples. These samples are divided into two groups. The first group includes 70% of samples used in the training phase of ANN, while the second group includes 30%, which is used in the testing phase of ANN. The distributing scenario of samples is performed because the three records in each implementation with the same irradiance and temperature

conditions are divided into two groups; two records in the first group and the other in the second. Thus, the first group includes 240 samples with 30 samples for each type of PV fault, and the second group includes 120 samples with 15 samples for each type of PV fault. The values of VIIT useful features differ from one implementation to another because the type of fault affecting the PV model differs.

The recorded samples of VIIT in the proposed PV model in a healthy state for the three irradiance conditions (500, 750, and 1000 W/m2) are plotted as the I-V curves in Figure (4.1, a, b, and c), respectively. The average I-load values are relatively high (10.2195A, 11.31623A, and 11.90527A) for all considered irradiance conditions. Thus, the generated power from the PV reaches the maximum limit because all branches and connections inside the PV module normally work without any losses.

The behavior of the average I-load values in the plotted in I-V curves mentioned in Figure (4.2) are repeated again in the PV model under the bad contact fault. The recorded values of I-load in all three considered irradiances are high (11.11989A, 12.92435A, and 13.60815A), respectively. Thus, the generated power from PV is slightly degraded according the growing in recorded current caused by the bad contact in the electrical connections within the internal connections of the PV module.

In the line-to-line fault condition, the average I-load values in the plotted I-V curves are mentioned in Figure (4.3) takes different behavior through slightly difference in current values in three considered irradiance conditions (10.20009A, 11.31623A, and 11.90527A). Thus, the generated power from PV fails to reflect the increasing in irradiance factor falls on the PV cells within the PV module.

For the short circuit fault condition in the PV module, three scenarios are considered for this fault condition, with different percentages of short circuits (25%, 50%, and 75%) verified in the PV module. The average I-load values for the plotted I-V curves in the proposed PV model under these three percentages of short circuit fault conditions are mentioned in Figure (4.4), Figure (4.5), and Figure (4.6), respectively. In this type of fault condition, the degradation in the generated power becomes more permanent, especially when the percentage of short circuits is increased. As a result, the average values of I-load in these three considered irradiances are (10.10377A, 11.30679A, 11.88195A), (7.431213A, 7.908687A, 8.275147A), and (3.923107A, 4.126613A, 4.30142A), respectively. Continuously, the generated power is reduced to (80%) from the healthy case in the first case of (25%) and goes down to (11%) in the third case of (75%) short circuit. This hard effect comes from the nature of the short circuit fault, which affects the overall electrical connection in the PV module because big parts of the cells inside the PV module are out of work.

For the Shadow fault condition in the PV module. The average I-load values for the plotted I-V curves in the proposed PV are mentioned in Figure (4.7). The recorded average values of the I-load in three considered irradiance conditions are (10.37266A, 12.92647A, 13.75915A), respectively. Thus, the generated power from PV equals is more than (92%) of the power in the healthy case. This small effect from that type of fault partially affects the PV's physical working by locking part of the sun's rays from falling on the face of the cell.

Finally, For the Open circuit fault condition in the PV module. The average I-load values in the plotted in I-V curves are mentioned in Figure (4.8). The recorded average values of the I-load in three considered

irradiance conditions are (10.34714A, 11.94345A, and 13.03869A), respectively. Thus, the generated power from the PV module is more than (82%) of the power in the healthy case. The shadow that falls on the solar panel has a significant impact on its productivity, depending on the extent of the shadow that is present on it.

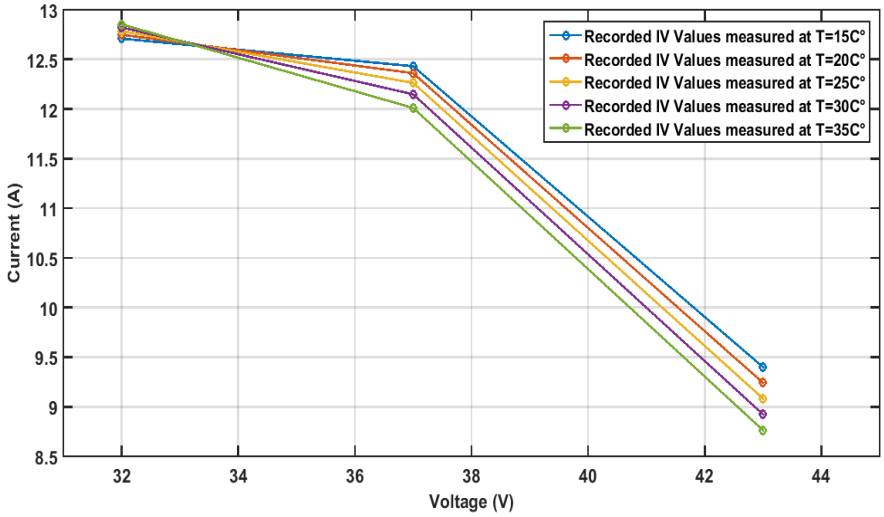

(a)

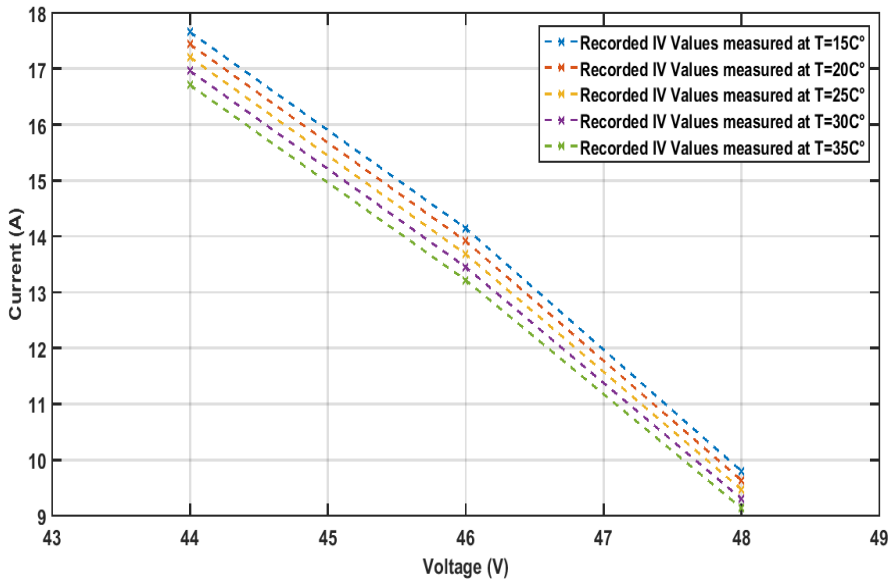

(b)

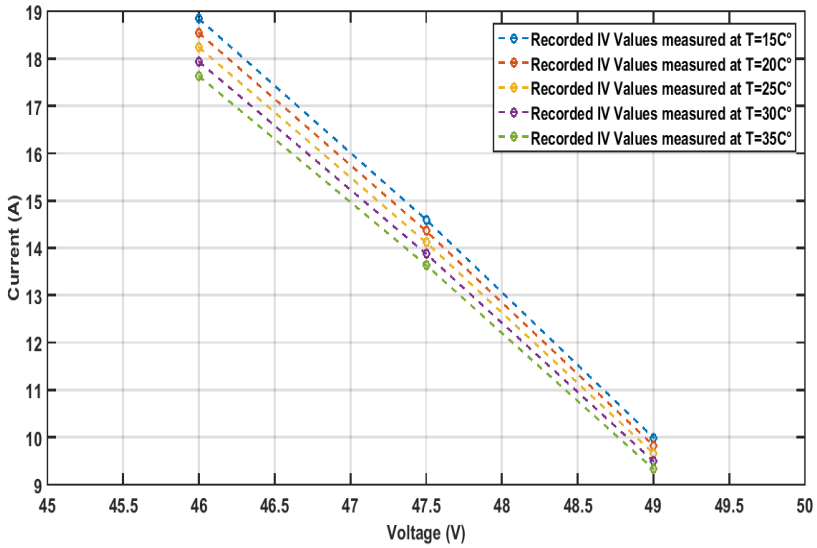

(c)

Figure (4.1): Measured I-V_{curves} of the Proposed PV Model using a Healthy State condition with three different loads, five temperature degrees, and three irradiance levels: (a) 500 W/m^2, (b) 750 W/m^2, and (c) 1000 W/m^2.

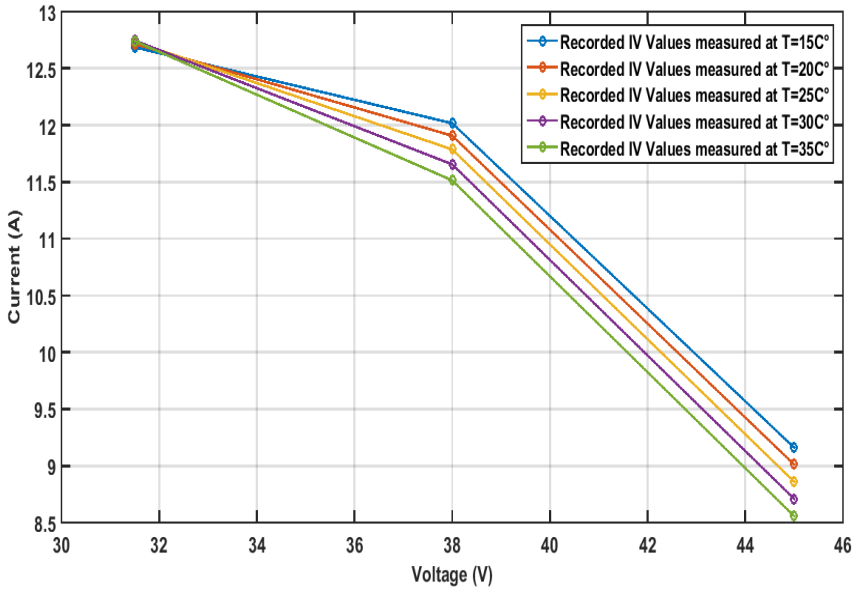

(a)

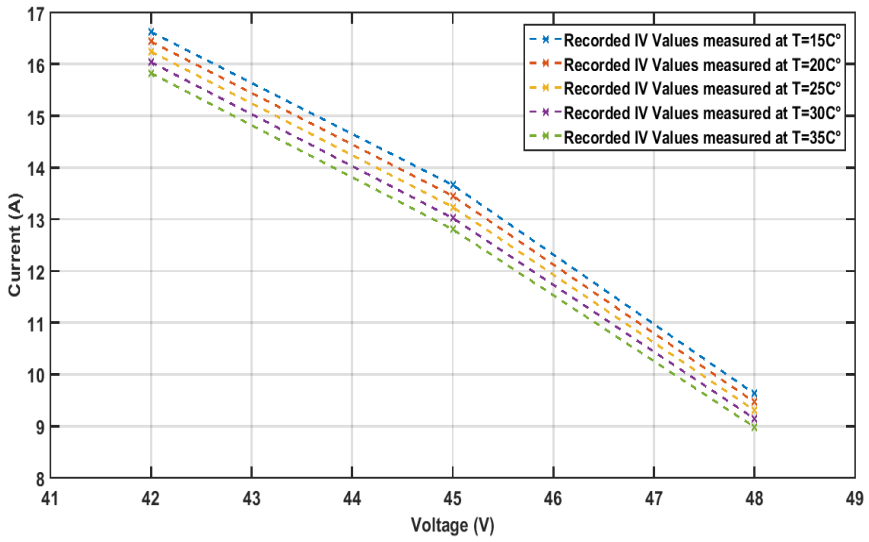

(b)

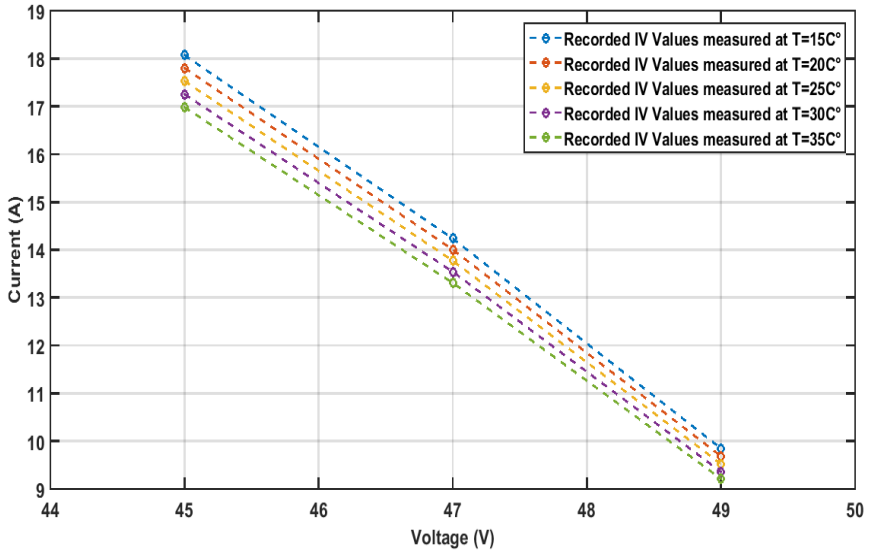

(c)

Figure (4.2): Measured I-V_{curves} of the Proposed PV Model using a Bad Contact Fault condition with three different loads, five temperature degrees, and three irradiance levels: (a) 500 W/m^2, (b) 750 W/m^2, and (c) 1000 W/m^2.

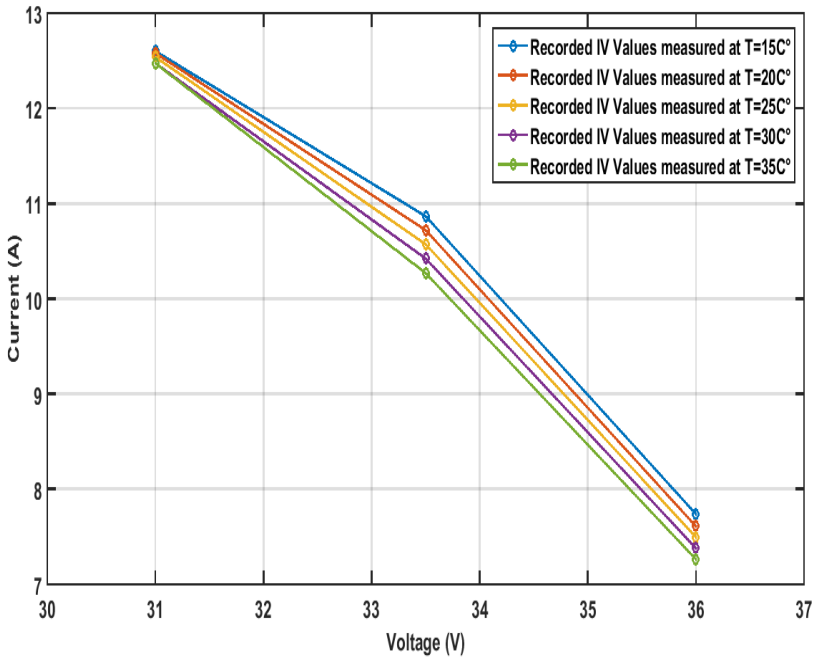
Recorded IV Values measured at T=15C°
Recorded IV Values measured at T=20C°
Recorded IV Values measured at T=25C°
Recorded IV Values measured at T=30C°
Recorded IV Values measured at T=35C°
Current (A)
Voltage (V)
13
12
11
10
9
8
7
30
31
32
33
34
35
36
37

(a)

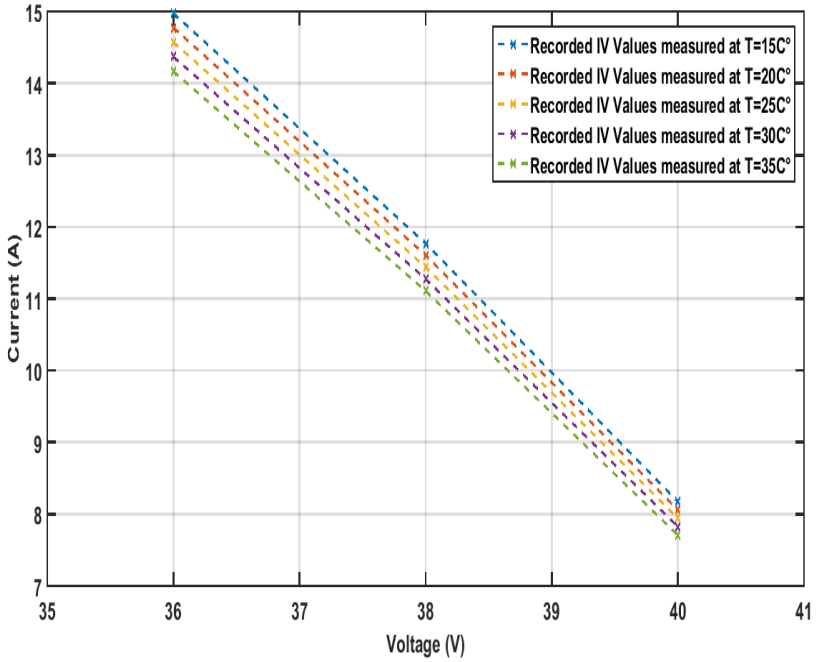
Recorded IV Values measured at T=15C°
Recorded IV Values measured at T=20C°
Recorded IV Values measured at T=25C°
Recorded IV Values measured at T=30C°
Recorded IV Values measured at T=35C°
Current (A)
Voltage (V)
15
14
13
12
11
10
9
8
7
35
36
37
38
39
40
41

(b)

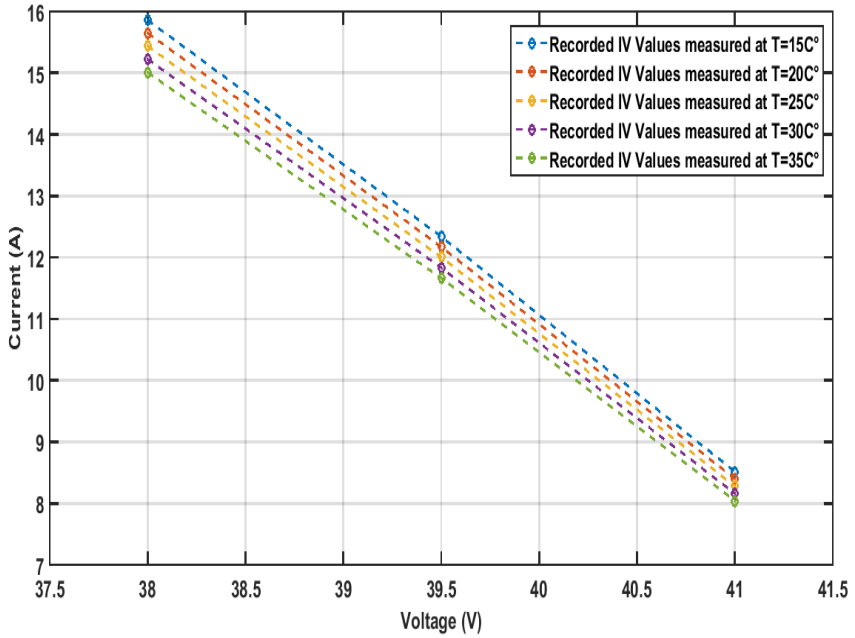

(c)

Figure (4.3): Measured I-V_{curves} of the Proposed PV Model using Line to Line Fault condition with three different loads, five temperature degrees, and three irradiance levels: (a) 500 W/m^2, (b) 750 W/m^2, and (c) 1000 W/m^2.

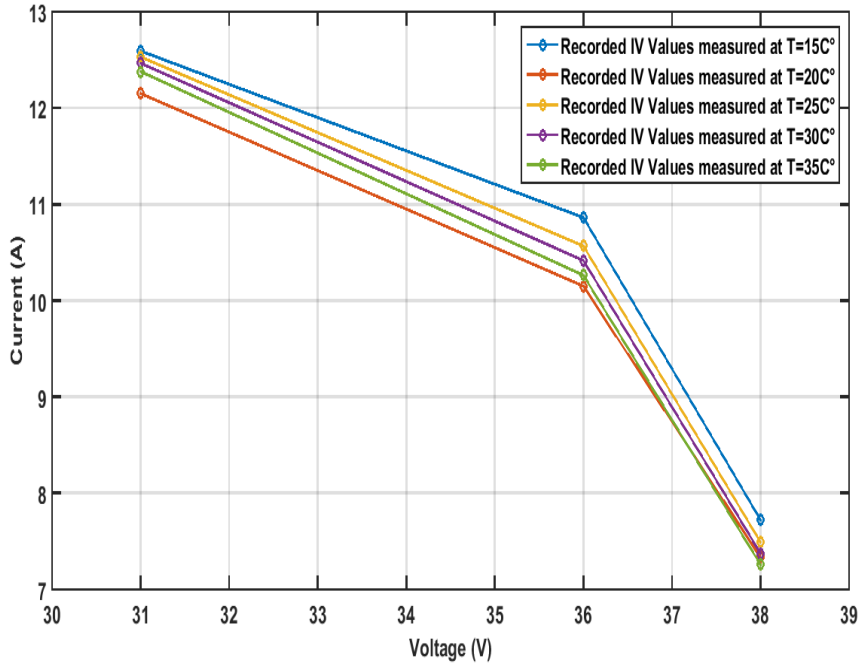

(a)

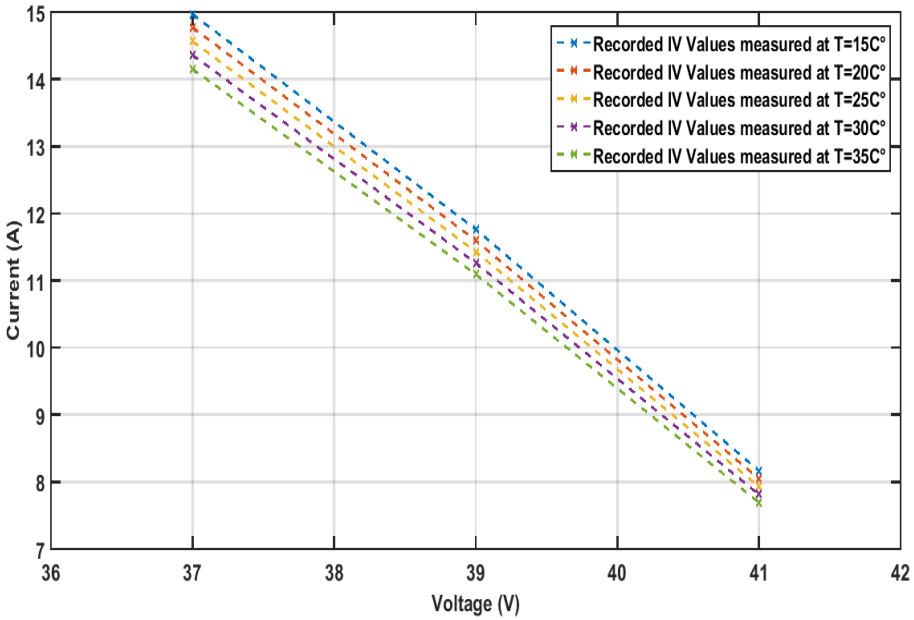

(b)

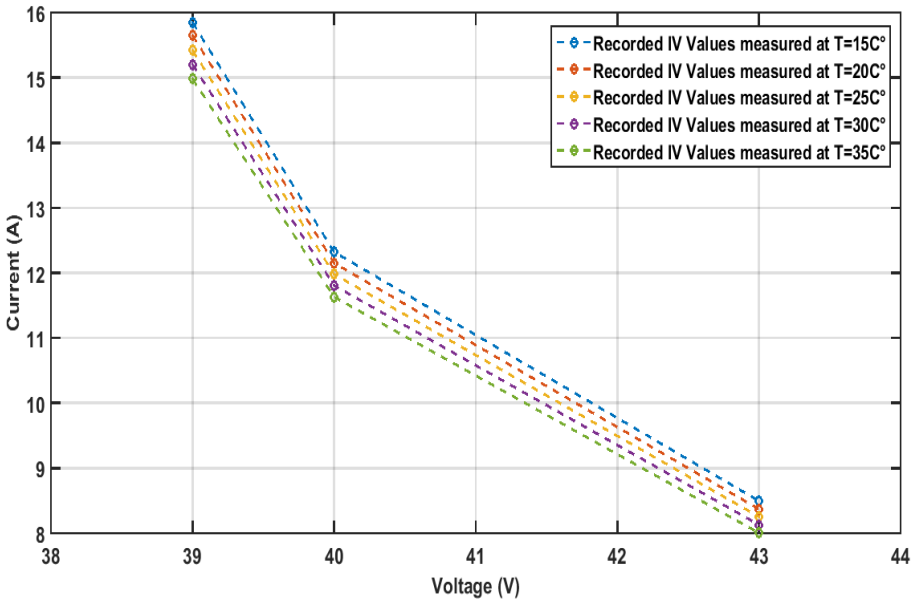

(c)

Figure (4.4): Measured I-V_{curves} of the Proposed PV Model using a 25% Short Circuit Fault condition with three different loads, five temperature degrees, and three irradiance levels: (a) 500 W/m^2, (b) 750 W/m^2, and (c) 1000 W/m^2.

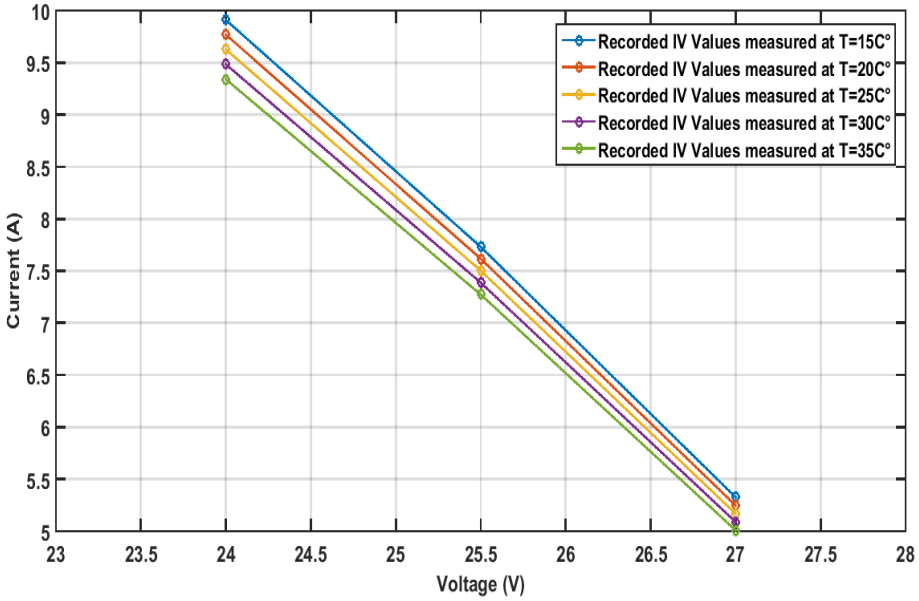
Recorded IV Values measured at T=15C°
Recorded IV Values measured at T=20C°
Recorded IV Values measured at T=25C°
Recorded IV Values measured at T=30C°
Recorded IV Values measured at T=35C°
Current (A)
Voltage (V)
10
9.5
9
8.5
8
7.5
7
6.5
6
5.5
5
23
23.5
24
24.5
25
25.5
26
26.5
27
27.5
28

(a)

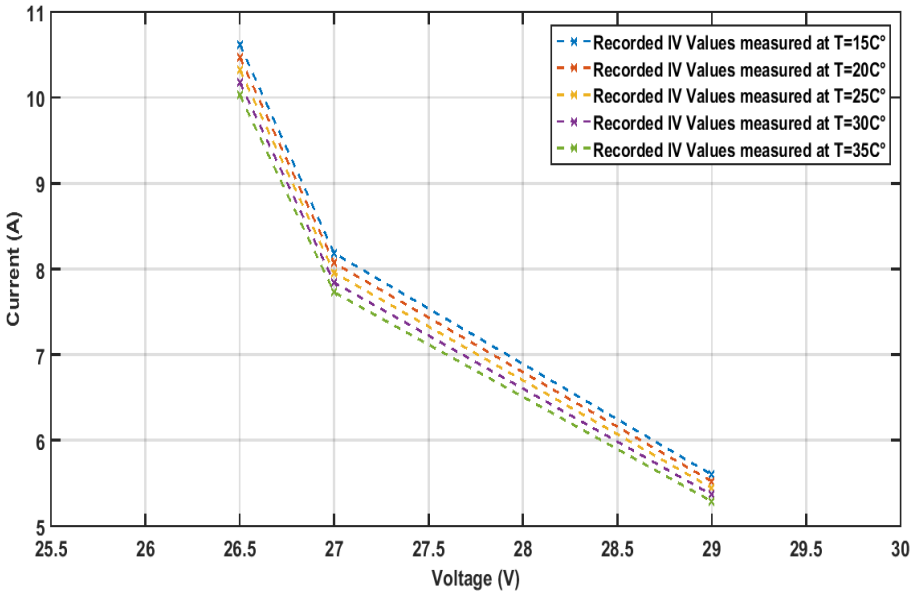
Recorded IV Values measured at T=15C°
Recorded IV Values measured at T=20C°
Recorded IV Values measured at T=25C°
Recorded IV Values measured at T=30C°
Recorded IV Values measured at T=35C°
Current (A)
Voltage (V)
11
10
9
8
7
6
5
25.5
26
26.5
27
27.5
28
28.5
29
29.5
30

(b)

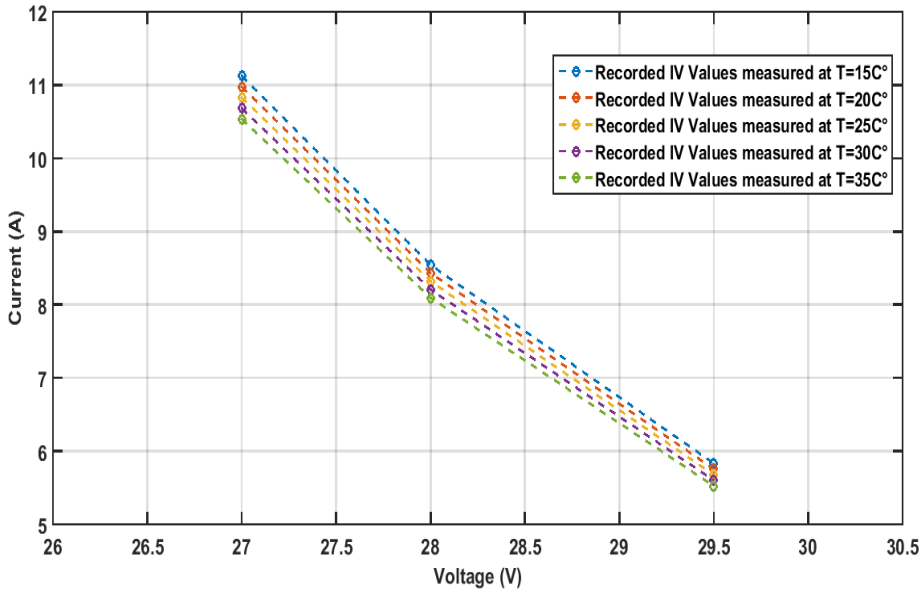

(c)

Figure (4.5): Measured I-V_{curves} of the Proposed PV Model using a 50% Short Circuit Fault condition with three different loads, five temperature degrees, and three irradiance levels: (a) 500 W/m^2, (b) 750 W/m^2, and (c) 1000 W/m^2.

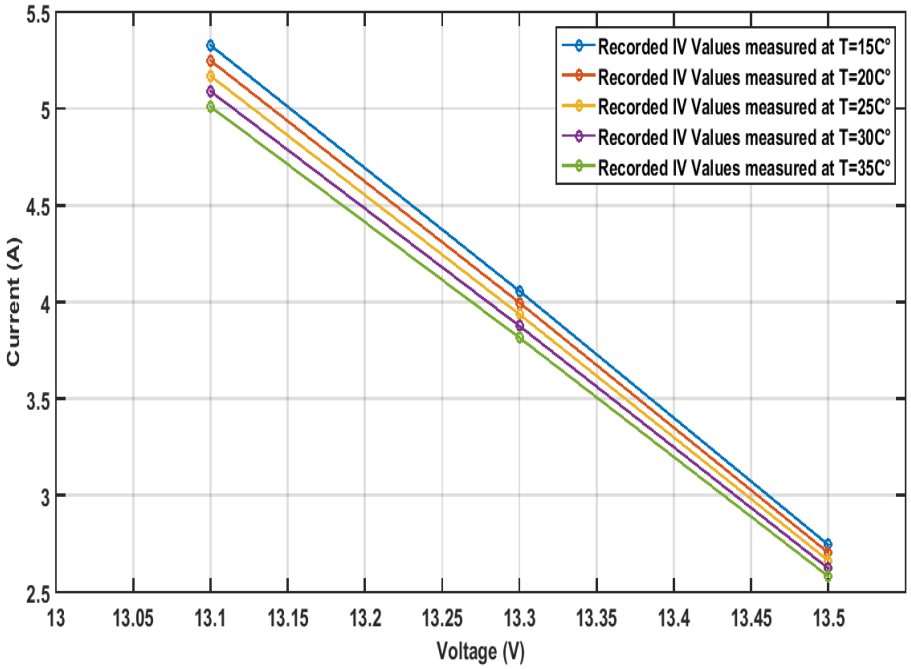

(a)

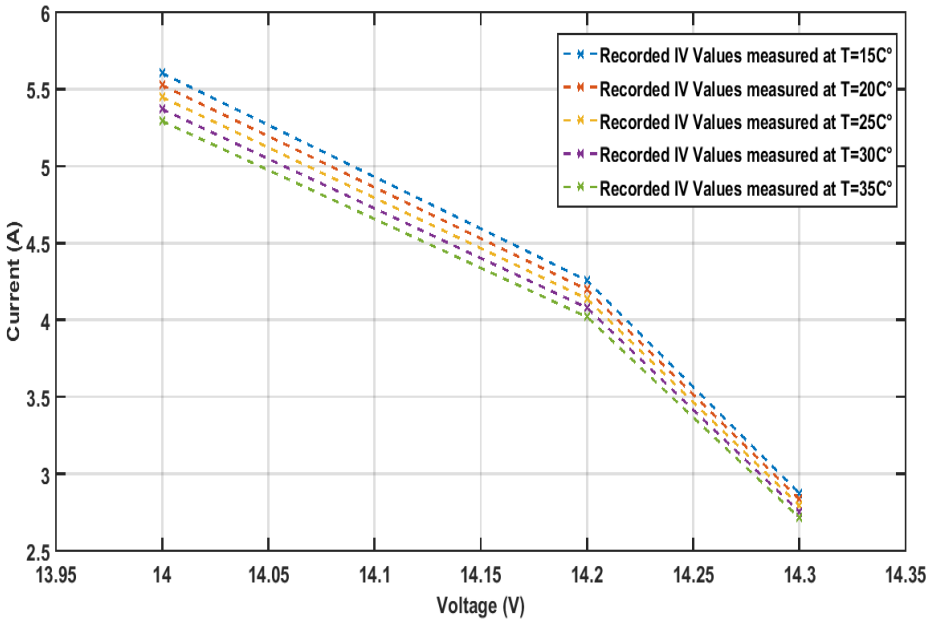

(b)

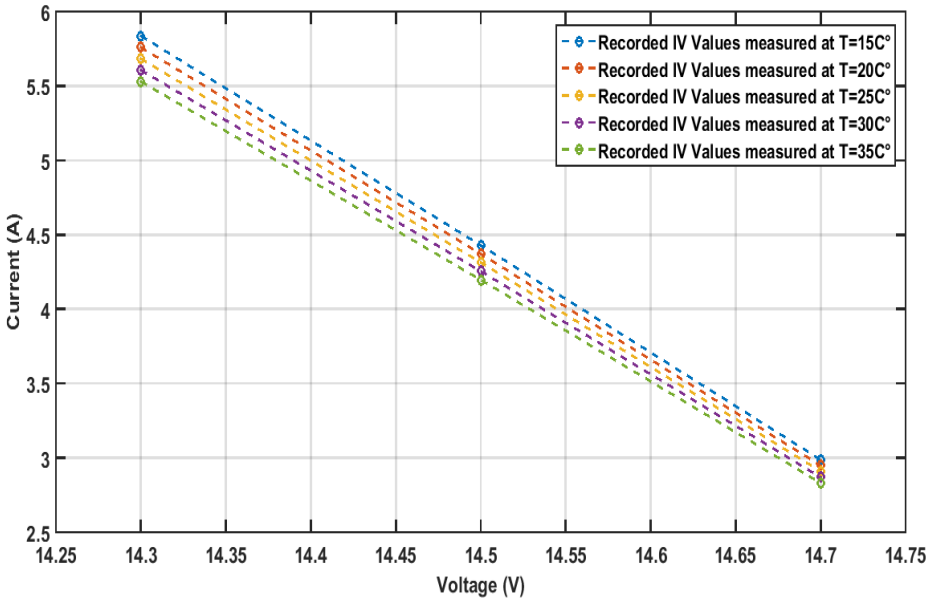

(c)

Figure (4.6): Measured I-V_{curves} of the Proposed PV Model using a 75% Short Circuit Fault condition with three different loads, five temperature degrees, and three irradiance levels: (a) 500 W/m^2, (b) 750 W/m^2, and (c) 1000 W/m^2.

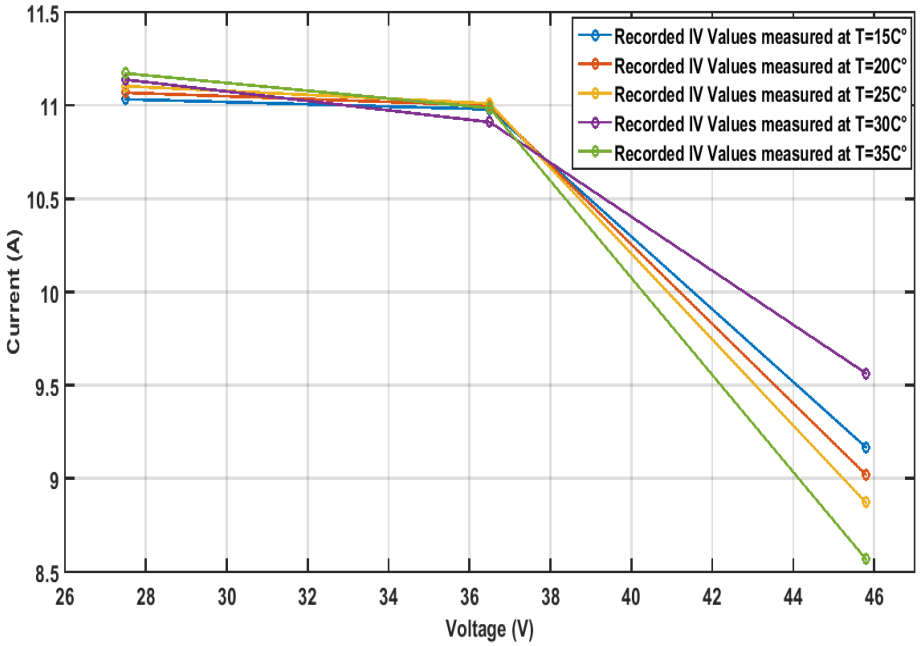
Recorded IV Values measured at T=15C°
Recorded IV Values measured at T=20C°
Recorded IV Values measured at T=25C°
Recorded IV Values measured at T=30C°
Recorded IV Values measured at T=35C°
Current (A)
Voltage (V)
11.5
11
10.5
10
9.5
9
8.5
26
28
30
32
34
36
38
40
42
44
46

(a)

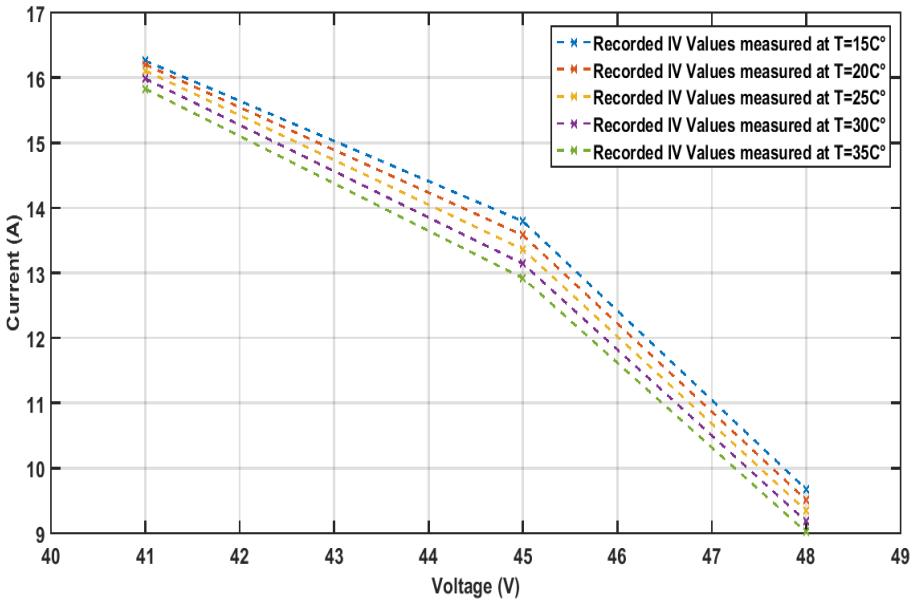
Recorded IV Values measured at T=15C°
Recorded IV Values measured at T=20C°
Recorded IV Values measured at T=25C°
Recorded IV Values measured at T=30C°
Recorded IV Values measured at T=35C°
Current (A)
Voltage (V)
17
16
15
14
13
12
11
10
9
40
41
42
43
44
45
46
47
48
49

(b)

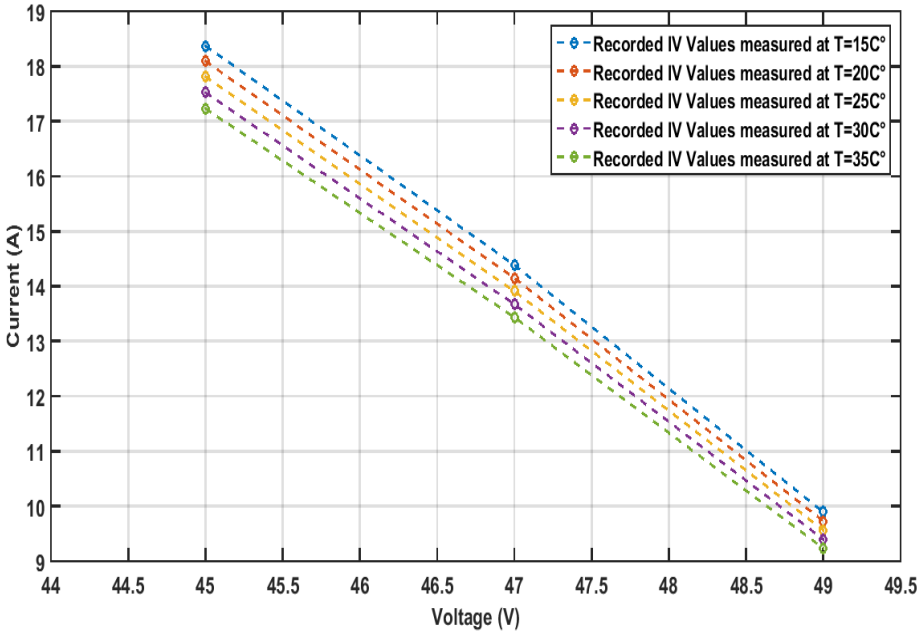

(c)

Figure (4.7): Measured I-V_{curves} of the Proposed PV Model using a Shadow Fault condition with three different loads, five temperature degrees, and three irradiance levels: (a) 500 W/m^2, (b) 750 W/m^2, and (c) 1000 W/m^2.

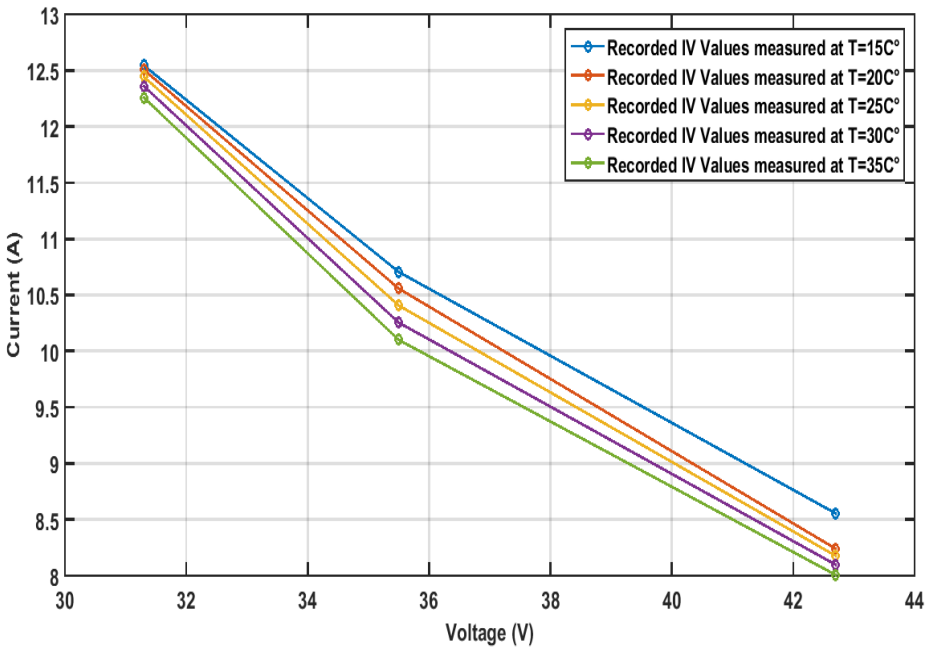

(a)

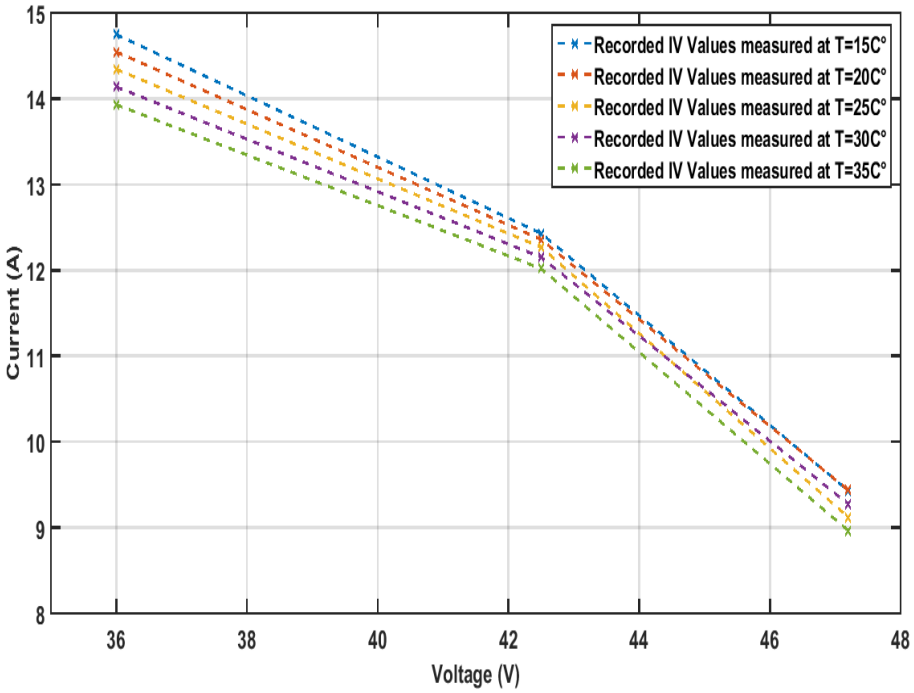

(b)

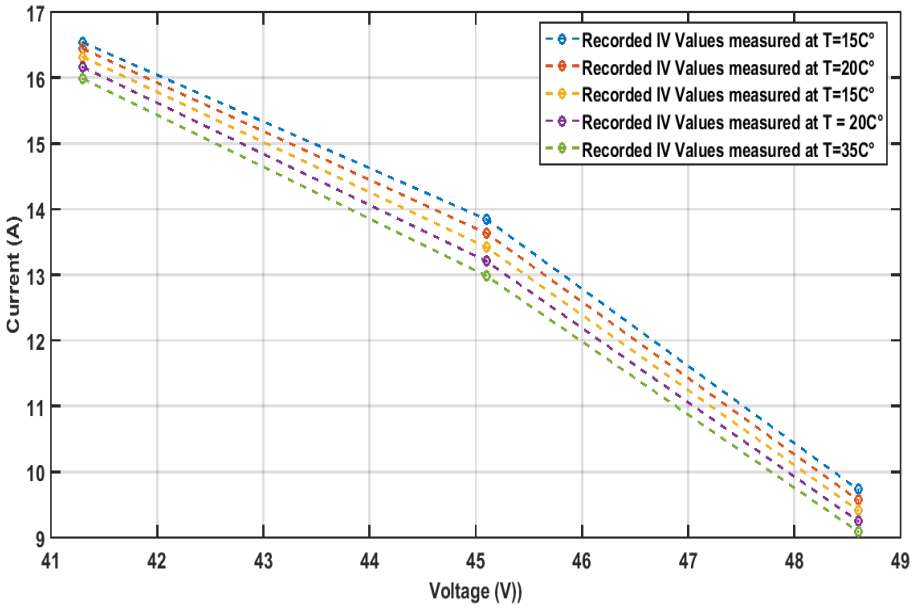

(c)

Figure (4.8): Measured I-V_{curves} of the Proposed PV Model using Open Circuit Fault condition with three different loads, five temperature degrees, and three irradiance levels: (a) 500 W/m^2, (b) 750 W/m^2, and (c) 1000 W/m^2.

4.3 Implementation of the Proposed ANN

The structure of the proposed ANN for diagnosing faults in the PV module is mentioned in Figure 3.4. This structure has four input neurons according to the VIIT useful features and eight output neurons according to the seven considered types of faults in addition to the healthy state. Also, there are several hidden layers between the input and output layers. These layers are inserted originally to expand the computation issue within the ANN to increase the accuracy of the final decision. Thus, the proposed ANN is implemented three times with three different numbers of neurons in the one hidden layer (25, 30, and 40) in each implementation.

4.3.1 Training Phase of the Proposed ANN

The training properties considered in the proposed ANN's training phase are the same in the three implementations. These properties are summarized in Table (4.1).

Table 4.1: Main Properties of the Proposed ANN

#	Title	Description/Value
1	Neural Network Type	Feed-forward neural network
2	Training Algorithm Name	Levenberg-Marquardt backpropagation
3	Maximum number of epochs to train	33000
4	Performance goal	1e-6
5	Maximum validation failures.	5000
6	Initial mu	1.00
7	Minimum performance gradient	1e-6

When the training process of the ANN is finished, the trained network must be evaluated to validate the performance of this network. In the MATLAB environment, four plotting diagrams are obtained automatically and describe the behaviour of this network during the training process. These diagrams are discussed separately in the following sections.

4.3.2 The Performance Diagram

As mentioned in Table 4.1, the maximum number of epochs considered in the training phase is 33000. The performance diagrams for

the three implementations mentioned in the previous section are shown in Figure (4.1.a, b, and c), respectively. In each diagram, the green line represents the validated fault, while the red line represents the test fault. The behavior of red and green curve. In Figure (4.1.a), the two curves go similarly, and there is convergence between them even at the minimum error point marked with a black circle and a vertical dashed line. While the same two curves in Figure (4.1, b, and c) go contiguous each other when the epochs counting of training is increased.

On the other hand, the blue line in these diagrams represents the flow of the training process. The behavior of this line in Figure (4.1.b and c) goes to the steady state value along with all the time spent for training. At the same time, there are the blue line reaching the state of stability in Figure (4.1.a).

The previous discussion about the three performance diagrams proves the quality of the first and second implementations according to the matching between the validated and tested line and the long period of steady state value for the training process.

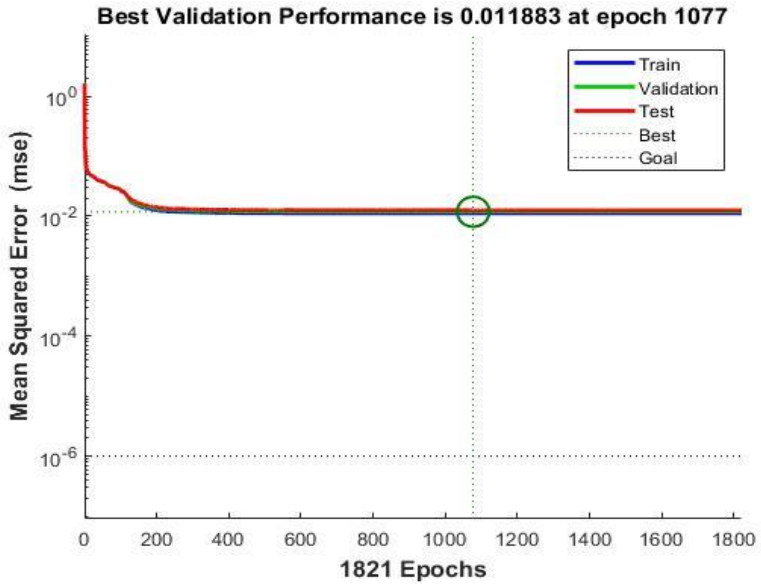

(a)

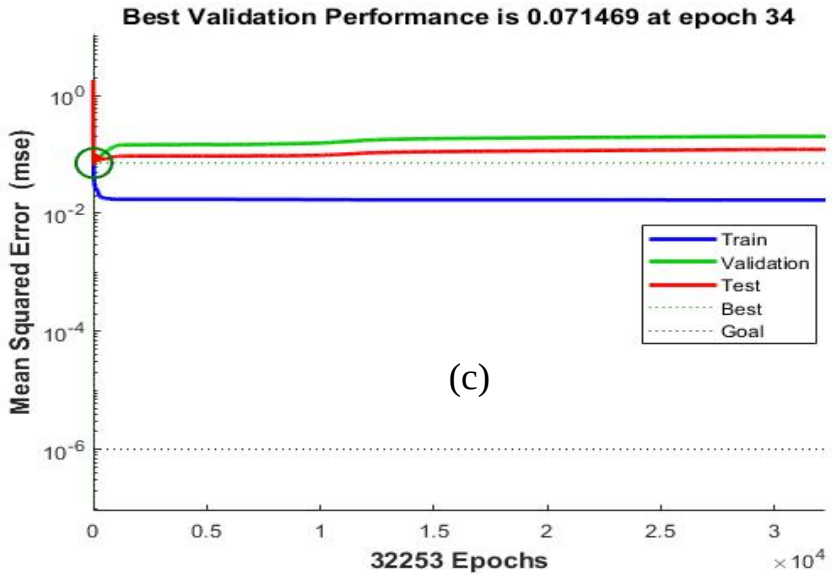

(c)

(b)

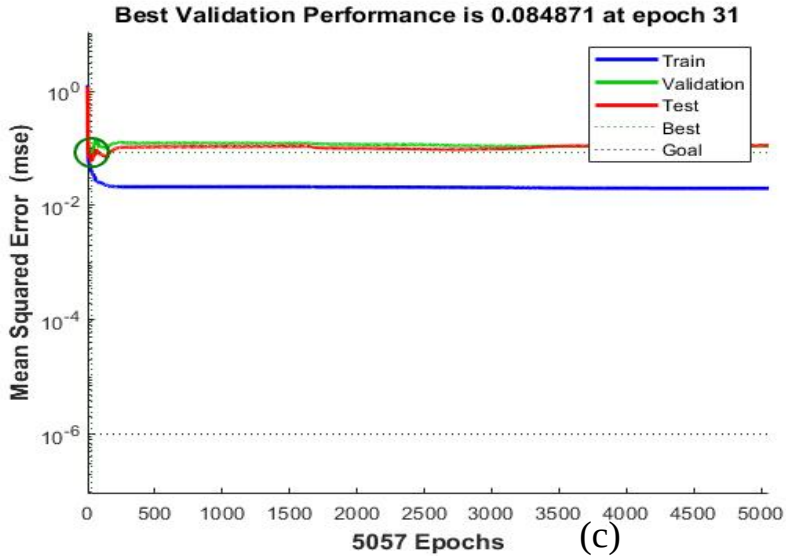

(c)

Figure 4.1: Performance Plotting Diagram of the Proposed ANN with; (a) 25, (b) 30, (c) 40 Neurons in the Hidden Layers.

4.3.3 Confusion Matrix Diagram

This section presents another evaluation diagram (the confusion matrix diagram) for the three considered implementations. This diagram acquires exceptional importance compared to the other evaluation diagram based on the fact that all the standard evaluation parameters, true positive (TP), true negative (TN), false positive (FP), and false negative (FN), are obtained in this diagram. The diagonal part in this matrix marked green contains the true positive elements with the correct fault classification value. In other words, this part handles the elements that the predicted and resulted faults are the same. Also, the diagonal cell in the lower right corner marked with blue contains the overall accuracy for all classification categories. The confusion matrix diagram for the three considered implementations is mentioned in Figure (4.2.a, b, and c), respectively

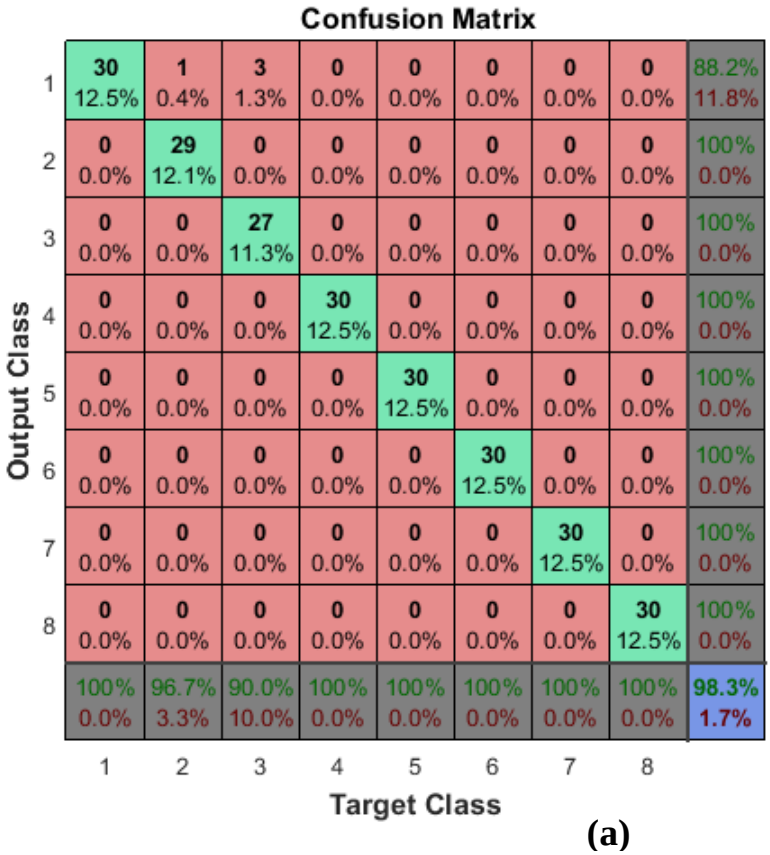

(a)

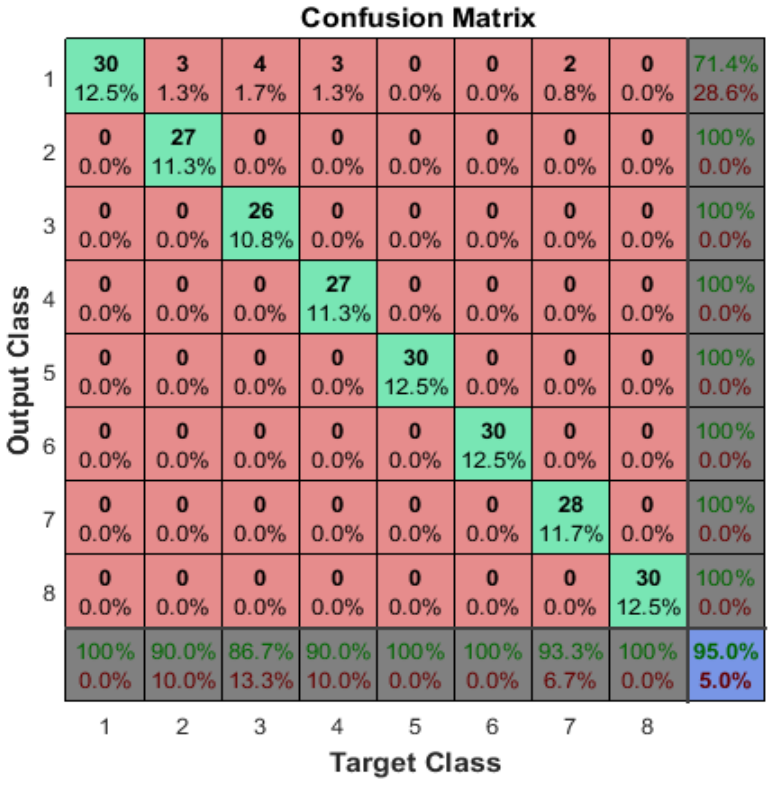

(b)

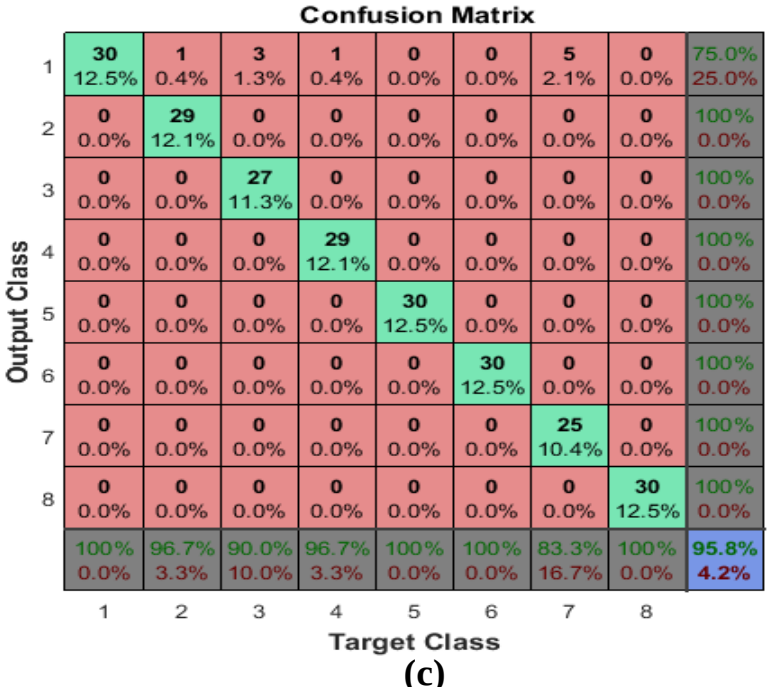

(c)

Figure 4.2: The Resulted Confusion Matrix Diagram of Three Implementations of the Proposed ANN in the training phase with; (a) 25, (b) 30, (c) 40 Neurons in the Hidden Layers.

The confusion matrix diagrams mentioned in Figure (4.2) result from the training phase of the proposed ANN, which handles 30 samples for each type of considered fault. The simulation results in Figure (4.2.a) for the ANN with 25 hidden layers get the maximum percentage of overall accuracy equal to (98.3%) compared to the other two matrix diagrams in Figure (4.2.b and c) with (95.0% and 95.8%), respectively. In order to calculate the accuracy and error we can use the following equation below:

Accuracy = PT+PN / PT+PN+FP+FN
Error = FP+FN / TP+TN+FP+FN
or
Error = 1 - Accuracy

The confusion matrix diagram is continuously determined again for the proposed ANN in the testing phase, which handles 15 samples for each type of considered fault. The confusion matrix diagrams, determined from the three implantations of the proposed ANN in the testing phase, are mentioned in Figure (4.3.a, b, and c), respectively. Tables 4.2, 4.3, and 4.4 show in the training phase the specific accuracy of each type of fault diagnosis. We note from the tables that the accuracy in fault diagnosis decreases as the number of hidden layers increases, and the reason for this is because the more hidden layers increase, the complexity of the artificial neural network increases, and the smart system proves the accuracy of 25 hidden layers. The error rate increases as the number of hidden layers increases

Table (4.2): The simulation results of the training phase with 25 hidden layers

Fault Name	No. of Training Samples	Predicated Faults by Proposed ANN			Accuracy %
		Correct fault	Wrong Faults	Details of wrong faults	
Healthy PV (FF1)	30	30	0		100%
Bad Contact (FF2)		29	1	1 FF1	96.7%
L-L fault (FF3)		27	3	3 FF1	90%
25% short (FF4)		30	0		100%
50%short (FF5)		30	0		100%
75%short (FF6)		30	0		100%
Shadow (FF7)		30	0		100%
Open circuit (FF8)		30	0		100%
Average Accuracy					98.3%

$$RMSE = \sqrt{\frac{(3+1)^2}{240}} = 0.258$$

Table (4.9): The simulation results of the training phase with 30 hidden layers

Fault Name	No. of Training Samples	Predicated Faults by Proposed ANN			Accuracy %
		Correct fault	Wrong Faults	Details of wrong faults	
Healthy PV (FF1)	30	30	0		100%
Bad Contact (FF2)		27	3	3 FF1	90%
L-L fault (FF3)		26	4	4 FF1	86.7%
25% short (FF4)		27	3	3 FF1	90%
50%short (FF5)		30	0		100%
75%short (FF6)		30	0		100%
Shadow (FF7)		28	2	2 FF1	93.3%
Open circuit (FF8)		30	0		100%
Average Accuracy					95%

$$RMSE = \sqrt{\frac{(3+4+3+2)^2}{240}} = 0.775$$

Table (4.4): The simulation results of the training phase with 40 hidden layers

Fault Name	No. of Training Samples	Predicated Faults by Proposed ANN			Accuracy %
		Correct fault	Wrong Faults	Details of wrong faults	
Healthy PV (FF1)	30	30	0		100%
Bad Contact (FF2)		29	1	1 FF1	96.7%
L-L fault (FF3)		27	3	3 FF1	90%
25% short (FF4)		29	1	1 FF1	96.7%
50%short (FF5)		30	0		100%
75%short (FF6)		30	0		100%
Shadow (FF7)		25	5	5 FF1	83.3%
Open circuit (FF8)		30	0		100%
Average Accuracy					95.8%

$$RMSE = \sqrt{\frac{(1+3+1+5)^2}{240}} = 0.646$$

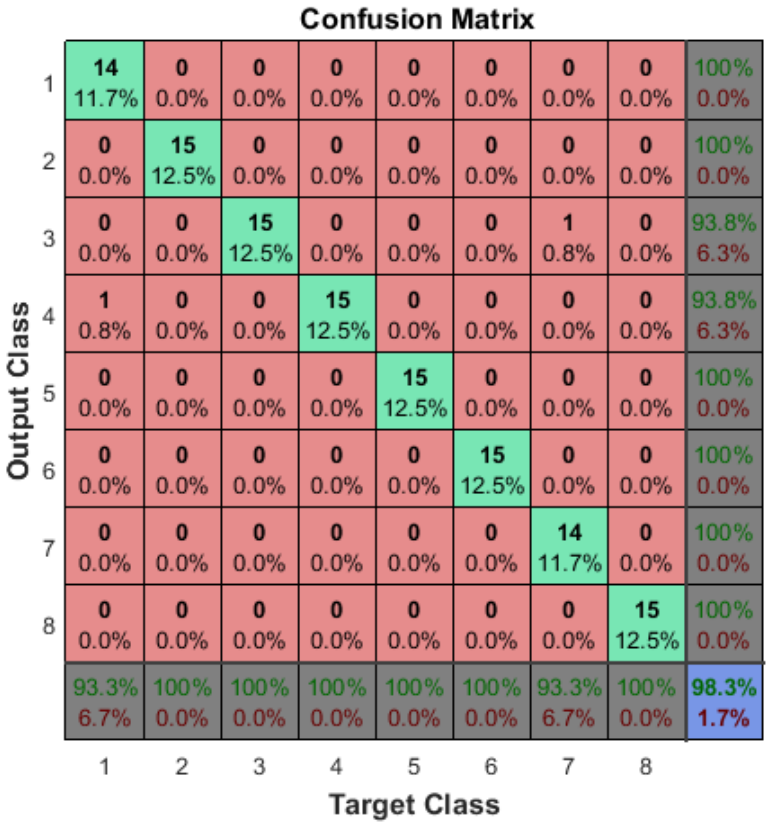
Confusion Matrix
Output Class
Target Class
1 2 3 4 5 6 7 8
14 11.7% | 0 0.0% | 0 0.0% | 0 0.0% | 0 0.0% | 0 0.0% | 0 0.0% | 0 0.0% | 100% 0.0%
0 0.0% | 15 12.5% | 0 0.0% | 0 0.0% | 0 0.0% | 0 0.0% | 0 0.0% | 0 0.0% | 100% 0.0%
0 0.0% | 0 0.0% | 15 12.5% | 0 0.0% | 0 0.0% | 0 0.0% | 1 0.8% | 0 0.0% | 93.8% 6.3%
1 0.8% | 0 0.0% | 0 0.0% | 15 12.5% | 0 0.0% | 0 0.0% | 0 0.0% | 0 0.0% | 93.8% 6.3%
0 0.0% | 0 0.0% | 0 0.0% | 0 0.0% | 15 12.5% | 0 0.0% | 0 0.0% | 0 0.0% | 100% 0.0%
0 0.0% | 0 0.0% | 0 0.0% | 0 0.0% | 0 0.0% | 15 12.5% | 0 0.0% | 0 0.0% | 100% 0.0%
0 0.0% | 0 0.0% | 0 0.0% | 0 0.0% | 0 0.0% | 0 0.0% | 14 11.7% | 0 0.0% | 100% 0.0%
0 0.0% | 0 0.0% | 0 0.0% | 0 0.0% | 0 0.0% | 0 0.0% | 0 0.0% | 15 12.5% | 100% 0.0%
93.3% 6.7% | 100% 0.0% | 100% 0.0% | 100% 0.0% | 100% 0.0% | 100% 0.0% | 93.3% 6.7% | 100% 0.0% | 98.3% 1.7%

(a)

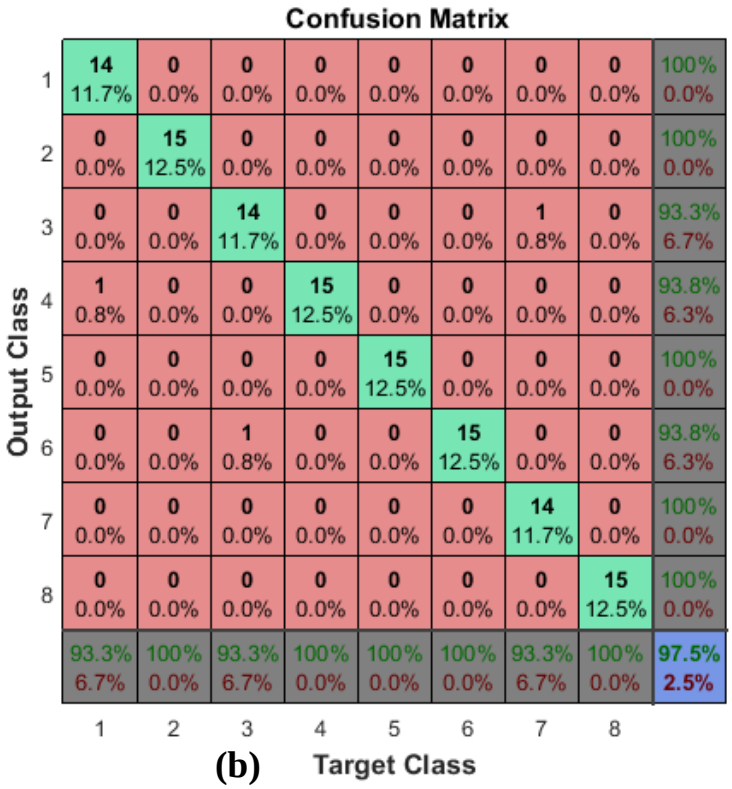
Confusion Matrix
Output Class
Target Class
1 2 3 4 5 6 7 8
14 11.7% | 0 0.0% | 0 0.0% | 0 0.0% | 0 0.0% | 0 0.0% | 0 0.0% | 0 0.0% | 100% 0.0%
0 0.0% | 15 12.5% | 0 0.0% | 0 0.0% | 0 0.0% | 0 0.0% | 0 0.0% | 0 0.0% | 100% 0.0%
0 0.0% | 0 0.0% | 14 11.7% | 0 0.0% | 0 0.0% | 0 0.0% | 1 0.8% | 0 0.0% | 93.3% 6.7%
1 0.8% | 0 0.0% | 0 0.0% | 15 12.5% | 0 0.0% | 0 0.0% | 0 0.0% | 0 0.0% | 93.8% 6.3%
0 0.0% | 0 0.0% | 0 0.0% | 0 0.0% | 15 12.5% | 0 0.0% | 0 0.0% | 0 0.0% | 100% 0.0%
0 0.0% | 0 0.0% | 1 0.8% | 0 0.0% | 0 0.0% | 15 12.5% | 0 0.0% | 0 0.0% | 93.8% 6.3%
0 0.0% | 0 0.0% | 0 0.0% | 0 0.0% | 0 0.0% | 0 0.0% | 14 11.7% | 0 0.0% | 100% 0.0%
0 0.0% | 0 0.0% | 0 0.0% | 0 0.0% | 0 0.0% | 0 0.0% | 0 0.0% | 15 12.5% | 100% 0.0%
93.3% 6.7% | 100% 0.0% | 93.3% 6.7% | 100% 0.0% | 100% 0.0% | 100% 0.0% | 93.3% 6.7% | 100% 0.0% | 97.5% 2.5%

(b)

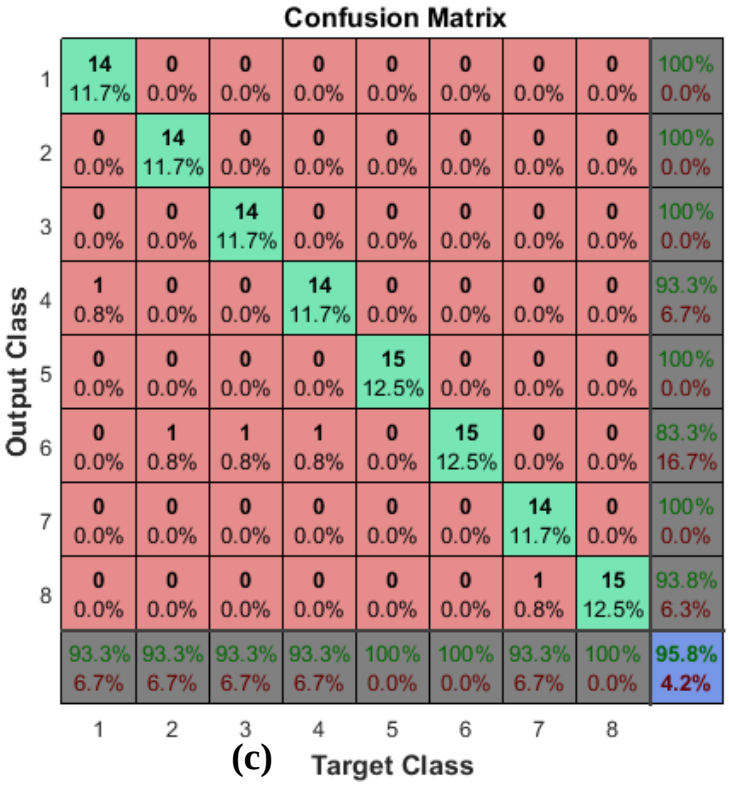

Figure 4.3: The Resulted Confusion Matrix Diagram of Three Implementation of the Proposed ANN in the testing phase with; (a) 25, (b) 30, (c) 40 Neurons in the Hidden Layers.

The same scenario in the training phase is repeated in the testing phase. The simulation results in three confusion matrix diagrams view that the best overall accuracy is recorded in the first implementation of the proposed ANN with 25 hidden layers. The maximum overall accuracy is (98.3%), while the second implementation with 30 hidden layers is (97.5%) and (95.8%) for the third implantation with 40 hidden layers. Tables 4.2, 4.3, and 4.4 show in the testing phase the specific accuracy of each type of fault diagnosis. We note from the tables that the accuracy in fault diagnosis decreases as the number of hidden layers increases, and the reason for this is because the more hidden layers increase, the complexity of the artificial neural network increases, and the smart system proves the

accuracy of 25 hidden layers. The error rate increases as the number of hidden layers increases.

Table (4.5): The simulation results of the testing phase with 25 hidden layers

Fault Name	No. of Testing Samples	Predicated Faults by Proposed ANN			Accuracy %
		Correct fault	Wrong Faults	Details of wrong faults	
Healthy PV (FF1)	15	14	1	1 Fault FF4	93.3%
Bad Contact (FF2)		15	0		100%
L-L fault (FF3)		15	0		100%
25% short (FF4)		15	0		100%
50%short (FF5)		15	0		100%
75%short (FF6)		15	0		100%
Shadow (FF7)		14	1	1 Fault FF3	93.3%
Open circuit (FF8)		15	0		100%
Average Accuracy					98.3%

$$RMSE = \sqrt{\frac{(1+1)^2}{120}} = 0.1826$$

Table (4.6): The simulation results of the testing phase with 30 hidden layers

Fault Name	No. of Testing Samples	Predicated Faults by Proposed ANN			Accuracy %
		Correct fault	Wrong Faults	Details of wrong faults	
Healthy PV (FF1)	15	14	1	1 Fault FF4	93.3%
Bad Contact (FF2)		15	0		100%
L-L fault (FF3)		14	1	1 Fault FF6	93.3%
25% short (FF4)		15	0		100%
50%short (FF5)		15	0		100%
75%short (FF6)		15	0		100%
Shadow (FF7)		14	1	1 Fault FF3	93.3%
Open circuit (FF8)		15	0		100%
Average Accuracy					97.5%

$$RMSE = \sqrt{\frac{(1+1+1)^2}{120}} = 0.274$$

Table (4.7): The simulation results of the testing phase with 40 hidden layers

Fault Name	No. of Testing Samples	Predicated Faults by Proposed ANN			Accuracy %
		Correct fault	Wrong Faults	Details of wrong faults	
Healthy PV (FF1)	15	14	1	1 Fault FF4	93.3%
Bad Contact (FF2)		14	1	1 Fault FF6	93.3%
L-L fault (FF3)		14	1	1 Fault FF6	93.3%
25% short (FF4)		14	1	1 Fault FF6	93.3%
50%short (FF5)		15	0		100%
75%short (FF6)		15	0		100%
Shadow (FF7)		14	1	1 Fault FF8	93.3%
Open circuit (FF8)		15	0		100%
Average Accuracy					95.8%

$$RMSE = \sqrt{\frac{(1+1+1+1+1)^2}{120}} = 0.456$$

4.3.4 The Error Histogram Diagram

This section presents another evaluating diagram called the error histogram diagram. This diagram takes the greatest importance in the evaluation process based on the fact that this diagram views the determined error between the resulted and predicated outputs. The histogram error diagram for the three implementations of the proposed ANN is mentioned in Figure (4.4.a, b, and c), respectively.

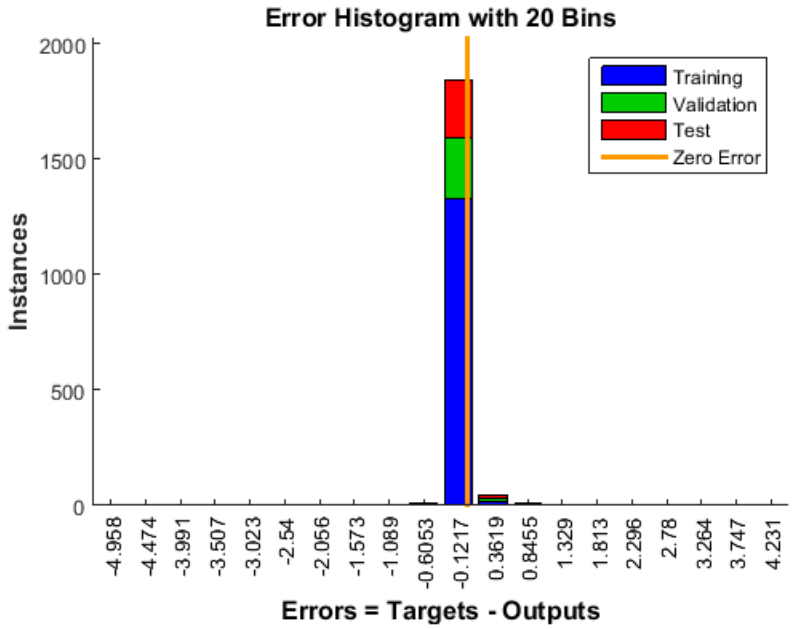
Error Histogram with 20 Bins
Training
Validation
Test
Zero Error
Instances
2000
1500
1000
500
0
-4.958
-4.474
-3.991
-3.507
-3.023
-2.54
-2.056
-1.573
-1.089
-0.6053
-0.1217
0.3619
0.8455
1.329
1.813
2.296
2.78
3.264
3.747
4.231
Errors = Targets - Outputs

(a)

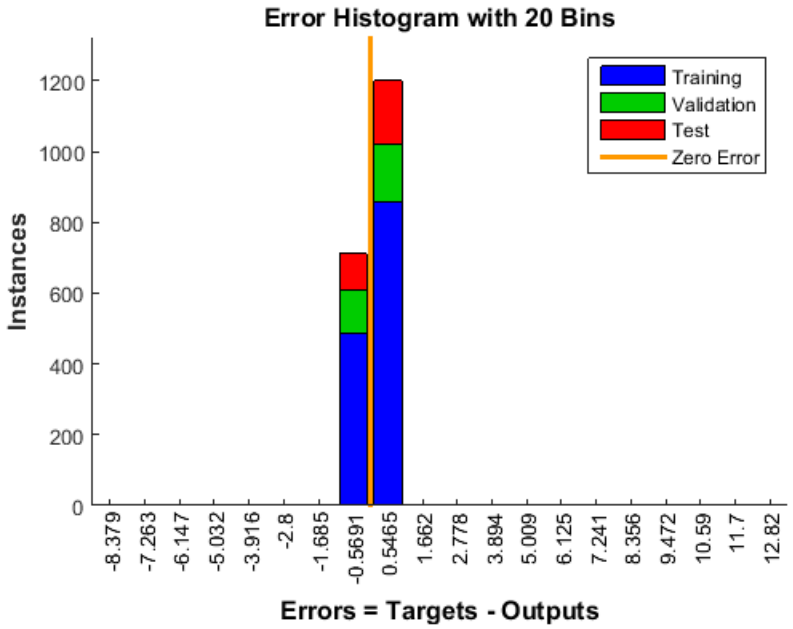
Error Histogram with 20 Bins
Training
Validation
Test
Zero Error
Instances
1200
1000
800
600
400
200
0
-8.379
-7.263
-6.147
-5.032
-3.916
-2.8
-1.685
-0.5691
0.5465
1.662
2.778
3.894
5.009
6.125
7.241
8.356
9.472
10.59
11.7
12.82
Errors = Targets - Outputs

(b)

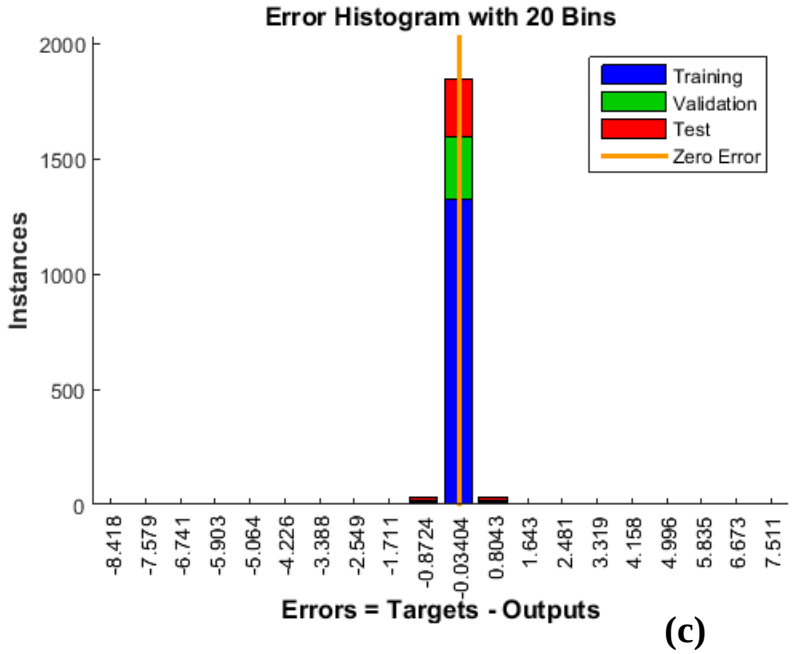

Figure 4.4: The Error Histogram Diagram of Three Implementation of the Proposed ANN in the training phase with; (a) 25, (b) 30, (c) 40 Neurons in the Hidden Layers.

The simulation results in these figures view that the most determined errors of tested, validated, and trained data in the three diagrams go nearest the zero-error vertical line marked with orange. This matching of more than 95% of components with zero value indicates the robustness of the proposed approach to generate important accuracy.

4.4 Comparison of the Proposed Approach

In this section, the simulation results, which are determined from the three implementations of the proposed ANN, are compared with the corresponding results from some well-known existing works of detecting different PV faults in the literature using ANN. The smart detecting technique of the PV faults, the number of faults, and the overall resulted in accuracy for the three existing works, in addition to the proposed approach, are illustrated in Table (4.8). The existing works for validation

are selected with the same classification technique ANN but with different types and numbers of PV faults.

The compared results are that the proposed approach scores overall accuracy equal to (98.3%) which is semi-equal to the maximum overall accuracy of one technique (98.2%) using the same smart technique for implementation. Applied to detect normal and four PV faults only compared to the proposed PV FDD approach, which successfully detected normal and seven PV faults, including all main types. Also, a short circuit fault is implemented with three different conditions. While the other existing work in the compared table successfully detected normal and nine PV faults, some main types of PV faults (line to line, bad contact, and open circuit) were not considered in the detected PV faults. Also, the recorded classification accuracy was less than one for the proposed FDD approach.

Finally, the study demonstrates that the Fuzzy Logic Controller successfully detects specified faults with consistently high accuracy (98.3% to 99.1%). However, to fully assess its reliability and performance, considerations like sample size, false positives/negatives, external factors, and comparison with other techniques are essential.

Table (4.8): Validation Results of Three Existing Techniques of PV Faults Detection and the Proposed Approach

#	Technique Name	Year	Description of Faults detected	Overall recorded Accuracy
1	ANN using (MLP) [9]	2020	1) Normal 2) Shading 50% of single cell 3) Shading 100% of single cell 4) Shading of a cell of the group 2-50% 5) Shading of a cell of the group 2-100% 6) Increase the resistance series 7) Shorted cell 8) Shading if six cells 9) Bypass diode reversed 10) defective bypass diode	97.2%
2	artificial intelligent nonlinear autoregressive exogenous neural network and Sugeno fuzzy inference [18]	2020	1) Normal 2) Open circuit degradation 3) Short circuit degradation 4) faulty MPPT 5) Partial shading conditions	98.2%
3	Fuzzy Logic controller [17]	2019	1) Short Circuit Fault 2) Open Circuit Fault 3) Partial Shading Bird or tree leaves dropping	99.1% 98.3% 99.1% 98.3%
4	The Proposed Approach of PV FDD Using ANN		1) Normal 2) Line to Line 3) Open Circuit 4) Bad Contact 5) Shadow 6) Short Circuit 25% 7) Short Circuit 50% 8) Short Circuit 75%	98.3% in the testing and training phases